Disclosure of potential conflict of interest: N. Hizawa is on the GlaxoSmithKline advisory board; has received research support from Astellas, AstraZeneca, Boehringer Ingelheim, GlaxoSmithKline, Kyorin, MSD, Novartis, and Chugai Pharmaceutical; and has received lecture fees from Astellas, AstraZeneca, Boehringer Ingelheim, GlaxoSmithKline, Kyorin, MSD, and Novartis. The rest of the authors declare that they have no relevant conflicts of interest.

REFERENCES

1. Rossios C, Pavlidis S, Hoda U, Kuo CH, Wiegman C, Russell K, et al. Sputum transcriptomics reveal upregulation of IL-1 receptor family members in patients with severe asthma. J Allergy Clin Immunol 2018;141:560-70.
2. FitzGerald JM, Bleecker ER, Nair P, Korn S, Ohta K, Lommatzsch M, et al. Benralizumab, an anti-interleukin-5 receptor α monoclonal antibody, as add-on treatment for patients with severe, uncontrolled, eosinophilic asthma (CALIMA): a randomised, double-blind, placebo-controlled phase 3 trial. Lancet 2016;388:2128-41.
3. Bleecker ER, FitzGerald JM, Chanez P, Papi A, Weinstein SF, Barker P, et al. Efficacy and safety of benralizumab for patients with severe asthma uncontrolled with high-dosage inhaled corticosteroids and long-acting beta2-agonists (SIROCCO): a randomised, multicentre, placebo-controlled phase 3 trial. Lancet 2016;388:2115-27.
4. Nair P, Wenzel S, Rabe KF, Bourdin A, Lugogo NL, Kuna P, et al. Oral glucocorticoid-sparing effect of benralizumab in severe asthma. N Engl J Med 2017;376:2448-58.
5. Tan LD, Bratt JM, Godor D, Louie S, Kenyon NJ. Benralizumab: a unique IL-5 inhibitor for severe asthma. J Asthma Allergy 2016;9:71-81.
6. Bauer M, Hackermuller J, Schor J, Schreiber S, Fink B, Pierzchalski A, et al. Specific induction of the unique GPR15 expression in heterogeneous blood lymphocytes by tobacco smoking. Biomarkers 2019;24:217-24.
7. Nguyen LP, Pan J, Dinh TT, Hadeiba H, O'Hara E III, Ebtikar A, et al. Role and species-specific expression of colon T cell homing receptor GPR15 in colitis. Nat Immunol 2015;16:207-13.

Available online August 11, 2020.
https://doi.org/10.1016/j.jaci.2020.08.004

Human immune disorder associated with homozygous hypomorphic mutation affecting MALT1B splice variant

To the Editor:

Identifying genetic mutations associated with human primary immune disorders provides unique opportunities to dissect the pathophysiologic relevance of genes for the human immune system and may guide therapeutic approaches for the affected patients.

T-cell antigen receptor (TCR) and B-cell antigen receptor ligation on lymphocytes triggers activation of canonic nuclear factor-κB (NF-κB) signaling, which is critical for mounting an adaptive immune response. The CARD11/CARMA1-BCL10-MALT1 (CBM) signaling complex acts as the gatekeeper for antigen receptor–induced NF-κB activation. In activated T cells, MALT1 serves a dual role as a scaffold and a protease. Whereas recruitment of the ubiquitin ligase TRAF6 to MALT1 triggers NF-κB signaling, the MALT1 protease cleaves distinct substrates to modulate T-cell effector functions. Germline mutations in all CBM components have been associated with a phenotypically diverse set of human primary immunodeficiencies termed *CBM-opathies*.[1] To date, 9 patients carrying a total of 6 different mutations in the *MALT1* gene that are linked to combined immune deficiency have been identified.[1,2] Importantly, all known mutations cause loss of function as a result of the absence or strong reduction of MALT1 protein expression. Here, we have described the first case of a severe immune syndrome caused by a homozygous hypomorphic mutation in the human *MALT1* gene.

A 19-year-old Turkish girl of parents who are first-degree cousins presented with a history of recurrent chronic purulent otitis and secondary poor hearing at admission. She was treated and hospitalized several times for bronchopneumonia. Physical examination resulted in diagnosis of a widespread seborrheic dermatitis on her scalp, psoriasis on her hand and foot extensor regions, severe warts on her hands, and bilateral axillary and cervical lymphadenomegaly. High-resolution chest tomography revealed superior segmental linear atelectasis with bronchiectasis in the lower lobe of the right lung. In the axillary and retropectoral regions, 2.7 × 12-mm conglomerate lymph nodes were identified. On abdominal ultrasonography, splenomegaly and grade 1 hydroureteronephrosis in the right kidney as well as multiple lymphadenopathies in the epigastric and paraaortic regions were found. An excisional biopsy revealed follicular hyperplasia of an enlarged lymph node, but malignancy was excluded. Scalp biopsies showed hyperplasia in squamous epithelium and psoriasis with perivascular lymphocyte infiltration in the dermis that was diagnosed as psoriasis with cutaneous symptoms.

Laboratory examinations (Table I[3,4]) revealed an IgA deficiency in the serum, whereas IgG levels were high owing to increased IgG1 and IgG3 levels. Specific antibody responses to tetanus and *Haemophilus influenzae* type B were normal. Hypocomplementemia for complement C3 and complement C4 was observed. Detection of autoantibodies and a positive direct Coombs test result established signs of autoimmunity. The relative numbers of $CD3^+$ T cells and $CD19^+$ B lymphocytes in the patient's peripheral blood were within the expected range (Table I and see Fig E1, *A* in this article's Online Repository at jacionline.org), but a change in $CD4^+/CD8^+$ T-cell ratio in the patient (~0.8:1) compared with in healthy controls (~2:1 ratio) indicated altered immune function (see Fig E1, *B*). There was a slight tendency toward more activated $CD69^+CD4^+$ T cells in the patient's peripheral blood (Fig E1, *C*). The patient's $CD3^+$ T cells were able to proliferate *in vitro* in response to PHA treatment (Fig E1, *D*).

Because the patient's clinical features indicated a primary immune deficiency with additional signs of autoimmunity, targeted next-generation sequencing was performed by using a primary immune deficiency research panel comprising 264 genes. We identified a heterozygous missense mutation c.2080A>G (p.Met694Val;M694V) in the *MEFV* gene, which is an autosomal recessive mutation associated with familial Mediterranean fever. The clinical pathology of familial Mediterranean fever with recurrent fever episodes is very distinct from what was observed in the patient, but some contribution cannot be completely excluded.[5] A single homozygous missense mutation, c.2418G>C (p.Glu806Asp;E806D), in the *MALT1* gene was identified (see Fig E2 in this article's Online Repository at jacionline.org). Sanger sequencing verified the homozygous *MALT1* c.2418G>C mutation in exon 17 of the patient, whereas her parents, who had no clinical symptoms, were heterozygous for the mutation (Fig 1, *A*). With *MALT1A* and *MALT1B* (Δexon 7) 2 splice variants exist, and transcripts for both isoforms were expressed in patient and control PBMCs (Fig 1, *B* and see Fig E3 in this article's Online Repository at jacionline.org). Thus, the *MALT1* c.2418G>C missense mutation leads to Glu806Asp (E806D) and Glu795Asp (E795D) substitution in MALT1A and MALT1B protein, respectively (Fig 1, *C*).[6] In contrast to all other known human MALT1 loss-of-function mutations, the MALT1 E806D/E795D mutant protein was

TABLE I. Laboratory and lymphocyte parameters

Parameter	Patient's value	Normal range of values
Serum immunoglobulin level (mg/dL)*		
IgA	<5	46.5-221
IgM	236	75.0-198.5
IgG	2930	830-1820
IgG1	2520	528-1384
IgG2	<37.6	147-610
IgG3	296	21-152
IgG4	<5.7	15-202
Antibody response		
Anti-tetanus IgG (IU/mL)	0.11	Normal
Anti-*H influenzae* B (μg/mL)	1.05	Normal
Complement level (mg/dL)		
C3	79	90-180
C4	6	10-40
Autoantibody		
ANA (titer)	1/320 (+)	Increased
C-ANCA (titer)	1/64 (+)	Increased
anti-MPO (RU/mL)	3	<20
Anti-PR3 (RU/mL)	38	<20
Direct Combs test	++	Negative
Lymphocyte count (%)†		
$CD3^+$	74	67.8-76.3
$CD3^+CD4^+$	42	58.7-70.6
$CD3^+CD8^+$	50	24.8-34.6
$CD19^+$	6	8.8-13.1

ANA, Antinuclear antibody; *c-ANCA*, cytoplasmic antineutrophil cytoplasmic antibody; *MPO*, myeloperoxidase; *PR3*, proteinase 3.
*Healthy Turkish children older than 16 years.[3]
†Healthy European/white females older than 20 years.[4]

expressed at wild-type (WT) levels in the patient's PBMCs (Fig 1, *D*). In line with this, MALT1B WT and E795D were expressed at equivalent levels on stable viral transduction in MALT1 knockout (KO) Jurkat T cells, whereas the previously identified MALT1B W569S mutant (corresponding to MALT1A W580S) was unstable but could be stabilized by an allosteric MALT1 inhibitor (see Fig E4, *A-C* in this article's Online Repository at jacionline.org).[7,8]

The *MALT1* c.2418G>C exchange occurs directly within the C-terminal evolutionarily conserved TRAF6 binding motif 2 (T6BM2) of MALT1 (Fig 1, *C* and see Fig E5 in this article's Online Repository at jacionline.org). Recruitment of TRAF6 via T6BMs to MALT1 is essential for NF-κB activation, but it is not directly connected to MALT1 protease activation in T cells.[6] Whereas MALT1A contains 2 functional T6BMs (T6BM1 and T6BM2), MALT1B lacks T6BM1 encoded by the alternatively spliced exon 7 and thus encodes only the T6BM2, which was mutated in the patient (Fig 1, *C*). Indeed, just like destruction of MALT1 T6BM by Glu/Ala (E/A) replacement,[6] the MALT1B E795D or MALT1A E806D patient mutation abolished or diminished TRAF6 binding, respectively. Stronger TRAF6 interaction of MALT1A was abrogated only with combined mutation of T6BM1 and T6BM2 (see Fig E6 in this article's Online Repository at jacionline.org). In the context of MALT1A, we then mutated the C-terminal T6BM2 in combination with the T6BM1, to show that both sites are required for full TRAF6 recruitment (see Fig E6).

To test whether the Glu/Asp replacement generates a hypomorphic variant that primarily affects activity of the shorter MALT1B isoform, we introduced Strep-tag II (ST)-tagged MALT1A WT, MALT1A E806D, MALT1B WT, and MALT1B E795D into MALT1 KO Jurkat T cells containing an NF-κB–dependent enhanced green fluorescent protein (EGFP) reporter. Stable transduction led to expression of all MALT1 variants at levels equivalent to that of endogenous MALT1 in the parental Jurkat T cells (Fig 1, *E* and F and see Fig E7, *A* and *B* in this article's Online Repository at jacionline.org). NF-κB activation was analyzed by detecting EGFP-positive cells by using flow cytometry after phorbol myristate acetate/ionomycin (P/I) or αCD3/CD28 antibodies to mimic TCR/CD28 costimulation and the cytokine TNF-α (see Fig E7, *C* and *D*). As expected, TNF-α–triggered NF-κB activation was not affected by MALT1 loss or mutations (Fig 1, *G* and *H*). Whereas the E806D mutation in MALT1A did not decrease NF-κB activation after P/I or TCR/CD28 costimulation, the identical E795D mutation in MALT1B abolished NF-κB activation in response to T-cell activation. Human blood $CD4^+$ T cells express levels of MALT1B that are approximately 5-fold higher than those of MALT1A.[6] To mimic such a scenario *in vitro*, we cotransduced MALT1 KO Jurkat T cells with untagged MALT1B E795D and increasing amounts of ST-tagged MALT1A WT or E806D (Fig 1, *I*). Indeed, low expression of MALT1A WT or E806D was unable to rescue defective TCR/CD28- and P/I-induced NF-κB activation in the presence of MALT1B E795D. MALT1A E806D was even more severely compromised in rescuing NF-κB signaling, demonstrating that the relative expression of MALT1A E806D and MALT1B E795D in patient T cells strongly influences the severity of the hypomorphic *MALT1* c.2418G>C loss-of-function mutation.

We have described a patient-derived homozygous *MALT1* c.2418G>C transversion, which leads to a unique hypomorphic MALT1 alteration that selectively disrupts signaling of the MALT1B isoform (Fig 1, *J*). The immune pathology is manifested by symptoms of immune deficiency such as chronic ear and bronchial infections and, at the same time, autoimmunity, as is evident from skin psoriasis, lymphadenopathies, and autoantibodies. We have provided evidence that the complex immune disorder may be linked to the relative expression of MALT1A and MALT1B in distinct immune cells. Defective activation in primarily MALT1B E795D–expressing T cells may explain the compromised patient immune responses and immune deficiencies. How the *MALT1* c.2418G>C mutation is associated with autoimmunity needs further investigations. Interestingly, psoriasis is driven by CARD14-MALT1 signaling in keratinocytes,[9] and we speculate that imbalanced MALT1A/MALT1B signaling in certain immune or nonimmune cells may result in overshooting immune or inflammatory responses causing autoimmunity.

Currently, the patient continues to experience recurrent ear infections despite prophylactic treatment with intravenous immunoglobulin replacement therapy, antibiotic prophylaxis, and *mycophenolate mofetil for preventing and treating autoimmunity.* The patient is enrolled for hematopoietic stem cell therapy, but because she is currently quarantined in her home in Eastern Turkey because of the COVID-19 pandemic, further clinical evaluations and basic research studies are not possible at this time.

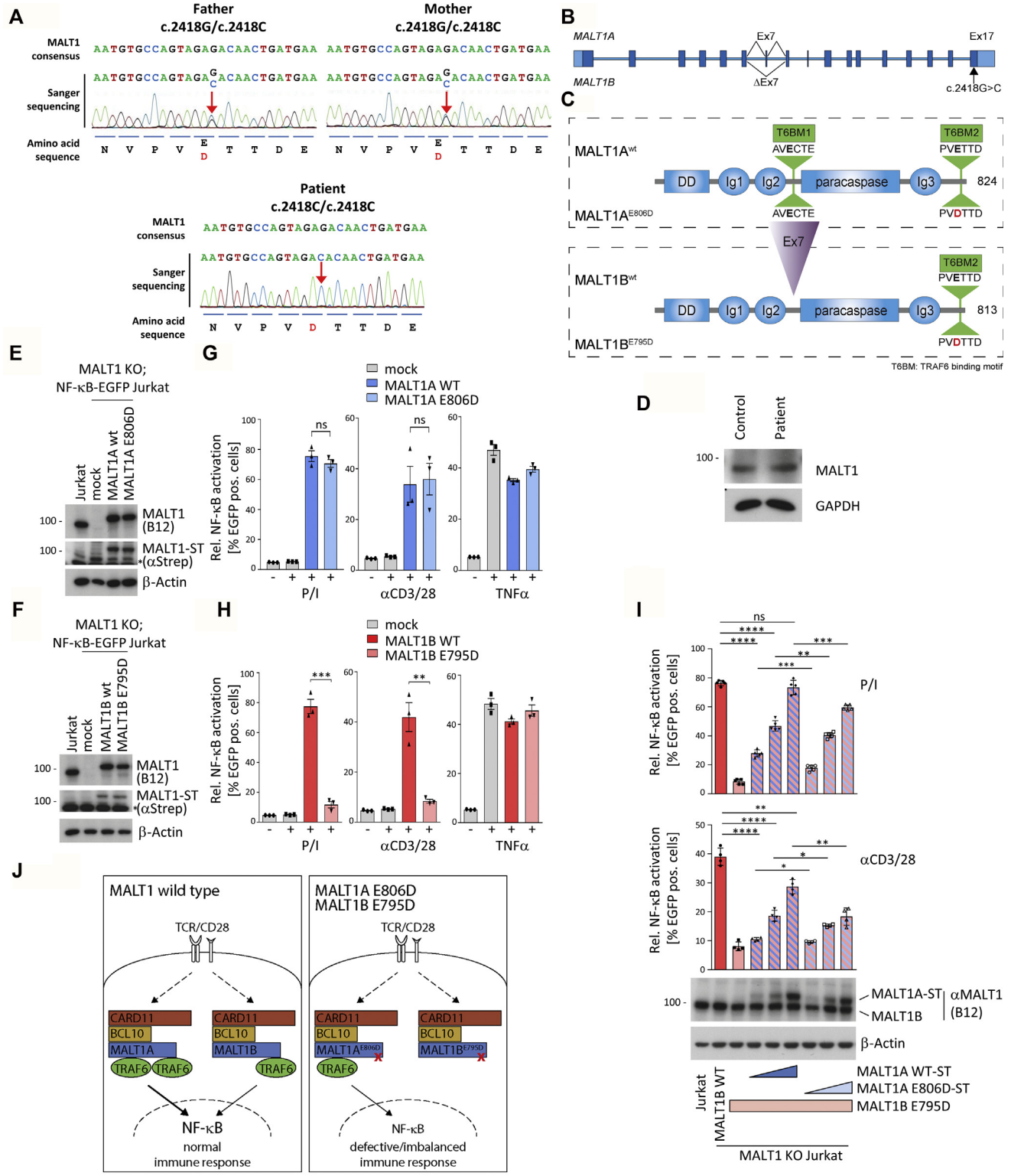

FIG 1. **A,** Identification of heterozygous and homozygous c.2418G>C mutation in the patient's parents and the patient. **B,** Scheme of the *MALT1* gene depicting alternatively spliced exon 7 in *MALT1A* and *MALT1B* and c.2418G>C mutation in exon 17. **C,** Structure of MALT1A and MALT1B showing TRAF6 binding motifs (T6BM) and the E806D or E795D mutation in T6BM2. **D,** MALT1 protein expression in blood PBMCs of the control and the patient. **E** and **F,** Expression of MALT1A and MALT1B WT and mutant proteins in transduced Jurkat T cells (asterisk marks an unspecific band). **G** and **H,** Quantification of NF-κB activation by EGFP-positive Jurkat T cells in MALT1A or MALT1B WT and mutant-expressing cells after P/I, αCD3/CD28, and TNF-α stimulation. **I,** Quantification of P/I- and αCD3/CD28-induced NF-κB activation in Jurkat T cells transduced with untagged MALT1B E795D and increasing concentrations of ST-tagged MALT1A WT or E806D. Protein expression was analyzed by Western blot. Data represent means ± SEMs of 3 (**G** and **H**), 4 (αCD3/CD28 [**I**]), or 5 (**I,** P/I) biologic replicates. ****$P \leq .0001$; ***$P \leq .001$; **$P \leq .01$; *$P \leq .05$; *ns*, not significant. **J,** Mechanistic model of the differential effects of the MALT1A E806D and the MALT1B E795D mutation on NF-κB signaling in T cells.

We thank Caspar Ohnmacht for technical support. Our work in Turkey was supported by the Jeffrey Modell Foundation. The work by D.K. was supported by the Deutsche Forschungsgemeinschaft (grants SFB 1054/A04 and SFB 1335/P07).

Necil Kutukculer, MD[a]*
Thomas Seeholzer, MSc[b]*
Thomas J. O'Neill, MSc[b]
Carina Graß, MSc[b]
Ayca Aykut, MD[c]
Neslihan Edeer Karaca, MD[a]
Asude Durmaz, MD[c]
Ozgur Cogulu, MD[c]
Guzide Aksu, MD[a]
Torben Gehring, PhD[b]
Andreas Gewies, PhD[b]
Daniel Krappmann, PhD[b]

From [a]the Department of Pediatric Immunology, Ege University Faculty of Medicine, and [c]the Department of Medical Genetics, Ege University Faculty of Medicine, Izmir, Turkey; and [b]the Research Unit Cellular Signal Integration, Helmholtz Zentrum München–German Research Center for Environmental Health, Neuherberg, Germany. E-mail: necil.kutukculer@ege.edu.tr. Or: daniel.krappmann@helmholtz-muenchen.de.

*These authors contributed equally to this work.

Disclosure of potential conflict of interest: D. Krappmann is a consultant for Monopteros Therapeutics, Boston. The rest of the authors declare that they have no relevant conflicts of interest.

REFERENCES

1. Lu HY, Bauman BM, Arjunaraja S, Dorjbal B, Milner JD, Snow AL, et al. The CBM-opathies-a rapidly expanding spectrum of human inborn errors of immunity caused by mutations in the CARD11-BCL10-MALT1 complex. Front Immunol 2018;9:2078.
2. Frizinsky S, Rechavi E, Barel O, Najeeb RH, Greenberger S, Lee YN, et al. Novel MALT1 mutation linked to immunodeficiency, immune dysregulation, and an abnormal T cell receptor repertoire. J Clin Immunol 2019;39:401-13.
3. Aksu G, Genel F, Koturoglu G, Kurugol Z, Kutukculer N. Serum immunoglobulin (IgG, IgM, IgA) and IgG subclass concentrations in healthy children: a study using nephelometric technique. Turk J Pediatr 2005;47:19-24.
4. Kverneland AH, Streitz M, Geissler E, Hutchinson J, Vogt K, Boës D, et al. Age and gender leucocytes variances and references values generated using the standardized ONE-Study protocol. Cytometry A 2016;89:543-64.
5. Schnappauf O, Chae JJ, Kastner DL, Aksentijevich I. The pyrin inflammasome in health and disease. Front Immunol 2019;10:1745.
6. Meininger I, Griesbach RA, Hu D, Gehring T, Seeholzer T, Bertossi A, et al. Alternative splicing of MALT1 controls signalling and activation of CD4(+) T cells. Nature Commun 2016;7:11292.
7. McKinnon ML, Rozmus J, Fung SY, Hirschfeld AF, Del Bel KL, Thomas L, et al. Combined immunodeficiency associated with homozygous MALT1 mutations. J Allergy Clin Immunol 2014;133:1458-62, 62 e1-7.
8. Quancard J, Klein T, Fung SY, Renatus M, Hughes N, Israel L, et al. An allosteric MALT1 inhibitor is a molecular corrector rescuing function in an immunodeficient patient. Nat Chem Biol 2019;15:304-13.
9. Zotti T, Polvere I, Voccola S, Vito P, Stilo R. CARD14/CARMA2 signaling and its role in inflammatory skin disorders. Front Immunol 2018;9:2167.

Available online August 25, 2020.
https://doi.org/10.1016/j.jaci.2020.07.034

METHODS

Informed consent was obtained from the patient and her parents.

Genomic exome library construction and targeted next-generation sequencing

Targeted next-generation sequencing was performed by using an Ion S5 sequencer (Thermo Fisher, Waltham, Mass). The Ion AmpliSeq Primary Immune Deficiency research panel (Thermo Fisher) comprising 264 genes was used, and analysis of mutations within 264 primary immune deficiency genes was done with Ion Reporter software. The potential functional impacts of the identified variants were assessed by using VarSome (Lausanne, Switzerland).

Purification of PBMCs

To purify PBMCs for flow cytometry and Western blot analysis, blood was drawn from donors into lithium-heparin tubes and centrifuged at 300 × *g* without brake for 10 minutes at room temperature (RT). Plasma (upper layer) was removed, and the buffy coat containing mononuclear cells (MNCs) and platelets (intermediate layer) was transferred and mixed with PBS to a total volume of 35 mL. Diluted sample was added carefully on top of 15 mL of Lymphoprep density gradient medium (StemCell Technologies, Cologne, Germany) and centrifuged (160 × *g* without brake for 20 minutes at RT) to purify the MNCs. Approximately 20 mL of platelets-containing supernatant was removed, and the remaining sample was centrifuged (at 350 × *g* without brake for 20 minutes at RT). Cells from the intermediate layer (MNCs) were separated, washed twice in 10 mL of buffer 1 (PBS containing 0.1% BSA and 2 mM EDTA [pH 7.4], sterile-filtered) (at 300 × *g* for 8 minutes at 4°C), and resuspended in medium (RPMI-1640, 10% FCS, 100 U/mL of penicillin/streptomycin, and 50 μM β-mercaptoethanol [all Thermo Fisher]). Protein expression in PBMCs was determined by Western blot using anti-MALT1 (B-12, Santa Cruz Biotechnology, Dallas, Tex) and anti–glyceraldehyde-3-phosphate dehydrogenase (GAPDH)–horseradish peroxidase (14C10, Cell Signaling Technology, Frankfurt, Germany) antibodies.

Immunologic phenotyping by flow cytometry

Lymphocyte populations were determined from single-cell PBMC suspensions stained with anti–CD3-APC (HIT31, 1:200, Biolegend, San Diego, Calif), anti–CD19-PEDazzle (SJ25C1, 1:200, Biolegend), anti–CD4-FITC (RPA-T4, 1:200, Biolegend), and anti–CD8-PECy5 (RPA-T8, 1:200, Biolegend). To investigate lymphocyte activation, anti–CD69-PECy5 (FN50, 1:200, Biolegend) was used. 2 × 10^5 PBMCs were washed twice with PBS and stained with Fixable Viability Dye eFluor 780 (1:1000; Thermo Fisher) for 30 minutes at 4°C to distinguish live from dead cells. The cells were washed with fluorescence-activated cell sorting buffer (3% FCS in PBS) and treated with anti-CD16/CD32 (Fc block; Thermo Fisher) for 20 minutes at RT. Cells were stained with fluorescent antibodies for 20 minutes at RT, washed with fluorescence-activated cell sorting buffer, and analyzed on an Attune Acoustic Focusing Cytometer (Thermo Fisher) or on an Fortessa Cytometer (Becton Dickinson, Franklin Lakes, NJ).

mRNA extraction and RT-PCR

mRNA was isolated (using an RNeasy Kit; Qiagen, Hilden, Germany) from 5 × 10^6 PBMCs; 400 ng of RNA was used for reverse transcription (Verso cDNA Synthesis Kit, Thermo Fisher). RT-PCR was performed by using LongAmp Taq DNA Polymerase (NEB, Frankfurt, Germany) with primers in flanking exons (the exon 6 primer ACCGAGACAGTCAAGATAGC and the exon 9/10 primer GACTTTGTCCTTTGCCAAAGG) detecting both isoforms MALT1A (146 bp) and MALT1B (113 bp). Next, 30 ng of cDNA or MALT1A/MALT1B plasmid DNA was used as a template. GAPDH/RNA polymerase II served as a control. PCR products were loaded on 2% to 3% agarose gel and visualized with UV light by using the gel documentation system (INTAS, Göttingen, Germany).

HEK293 cell transfection and MALT1-TRAF6 interaction

HEK293 cells were grown in Dulbecco modified Eagle medium (Thermo Fisher) supplemented with 10% FCS and 100 U/mL of penicillin/streptomycin; transfection of HA-TRAF6 (pEF vector) and MALT1-FlagStrepII constructs (pHAGE vector) was performed by using calcium phosphate precipitation. To study MALT1-TRAF6 interaction, cells were lysed in coimmunoprecipitation buffer (25 mM HEPES [pH 7.5], 150 mM NaCl, 0.2% NP-40, 10% glycerol, 1 mM dithiothreitol, 10 mM sodium fluoride, 8 mM β-glycerophosphate, 300 μM sodium vanadate, and protease inhibitor cocktail [Roche, Basel, Switzerland]) and subjected to Streptactin-pulldown (Strep-PD) using Strep-Tactin sepharose beads (IBA, Göttingen, Germany), and TRAF6-MALT1 binding was analyzed by Western blot.

Lentiviral transduction of Jurkat T cells

Jurkat T-cell lines were grown in RPMI-1640 medium supplemented with 10 % FCS and 100 U/mL penicillin/streptomycin. To generate stable MALT1-expressing cell lines, MALT1 KO;NF-κB-EGFP Jurkat T cells[E1] were lentivirally transduced with constructs in which MALT1A, MALT1A E806D, MALT1B, and MALT1B E795D were cloned into pHAGE-hΔCD2-T2A backbone vector. For this, lentiviruses were produced in HEK293T cells. In brief, 2 × 10^6 HEK293T cells were seeded in a 10-cm^2 dish in 8 mL of Dulbecco modified Eagle medium 1 day before transfection. The following day, HEK293T cells were transfected with 1 μg of the lentiviral envelope plasmid pMD2.G (Addgene catalog no. 12259; a gift of D. Trono), 1.5 μg of the packaging vector psPAX2 (Addgene catalog no. 12260; a gift from D. Trono), and 2 μg MALT1 transfer plasmid (pHAGE-hΔCD2-T2A-MALT1-StrepTagII) by using X-tremeGENE HP DNA Transfection Reagent (Roche) according to the manufacturer's instructions. After 3 days, the supernatant containing the virus particles was removed and sterile-filtered (0.45 μM) before addition of virus with 8 μg/mL of polybrene (Sigma Aldrich, St Louis, Mo) to 5 ×10^5 MALT1-deficient Jurkat T cells. After 24 hours, the cells were washed with PBS (3 times) and resuspended in 1 mL of fresh RPMI-1640 medium. After 2 weeks, transduction efficiency was assessed by analyzing surface expression of hΔCD2 in flow cytometry with anti–CD2-APC (RPA-2.10, 1:400, Invitrogen, Carlsbad, Calif). Western blots after transfection or transduction were carried out by using anti-MALT1 (B-12; Santa Cruz Biotechnology), anti-β-Actin (C4, Santa Cruz Biotechnology), anti-HA (12CA5; HMGU, Munich, Germany), and anti-StrepMAB–horseradish peroxidase (IBA).

NF-κB–EGFP reporter analyses in Jurkat T cells

MALT1 KO;NF-κB reporter Jurkat T cells that had been stably transduced with mock or different MALT1 constructs were stimulated with phorbol myristate acetate (200 ng/mL) and ionomycin (300 ng/mL) (P/I) (both Merck, Darmstadt, Germany), αCD3 (0.3 μg)/αCD28 (1 μg) antibodies in presence of anti-murine IgG1 (0.5 μg) and IgG2a (0.5 μg) (all BD Bioscience, Heidelberg, Germany), or TNF-α (20 ng/mL, Biomol, Hamburg, Germany) for 5 hours. EGFP expression was determined by flow cytometry, and quantification was done by gating on EGFP-positive cells.

REFERENCE

E1. Gehring T, Erdmann T, Rahm M, Graß C, Flatley A, O'Neill TJ, et al. MALT1 Phosphorylation controls activation of T lymphocytes and survival of ABC-DLBCL tumor cells. Cell Rep 2019;29:873-88.e10.

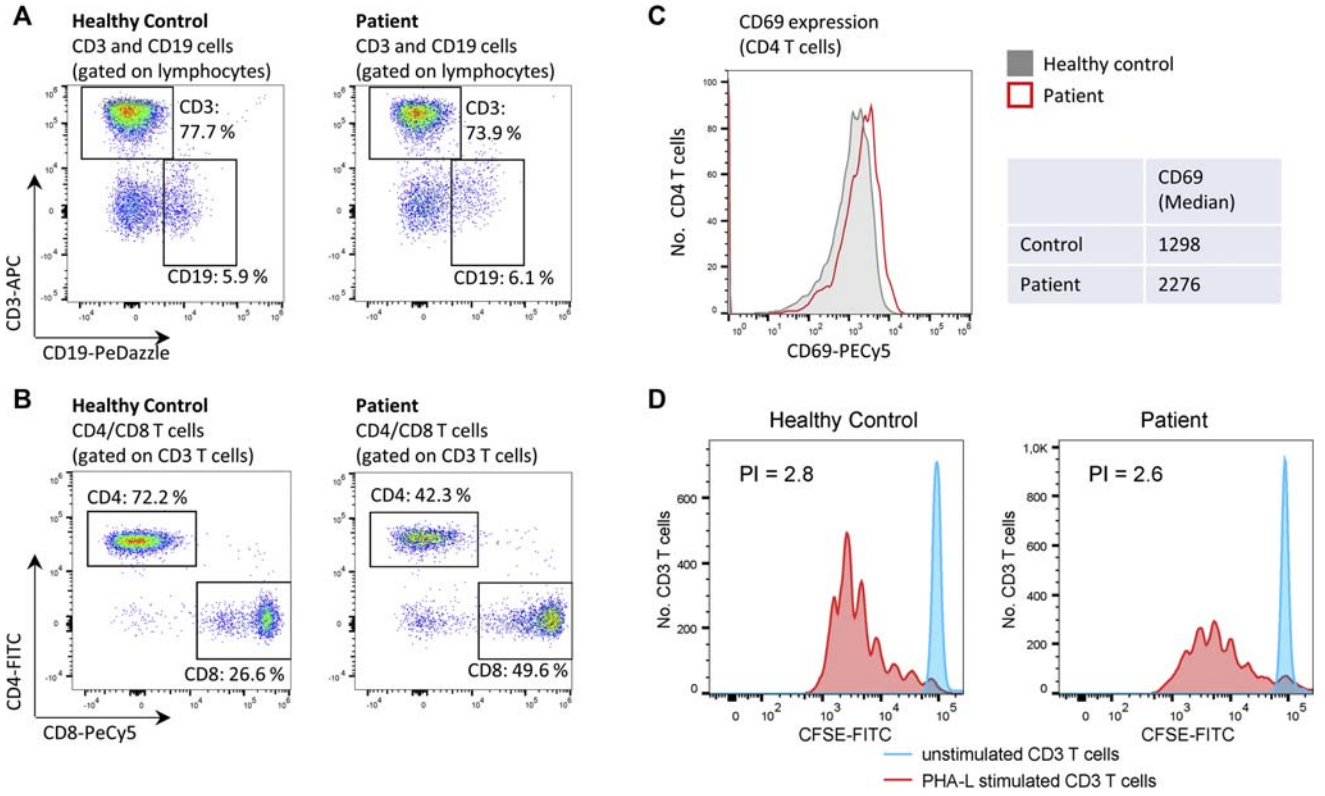

FIG E1. A, Fluorescence-activated cell sorting of $CD3^+$ T cells and $CD19^+$ B cells in blood PBMCs from the female patient and a healthy control. **B,** Fluorescence-activated cell sorting analyses of $CD4^+/CD8^+$ T-cell ratio in peripheral $CD3^+$ T cells from the blood of our patient and the control. **C,** Histogram comparing expression of activation marker CD69 on blood $CD4^+$ T cells in a healthy control and in the patient. **D,** Histogram graphics of unstimulated and PHA-L–stimulated $CD3^+$ T cells (gated on CD3-APC) representing intact *in vitro* T-lymphocyte proliferation response by the carboxyfluorescein succinimidyl ester (CFSE)–fluorescence-activated cell sorting (FACS) method of samples from healthy control and patient. The proliferation index (PI) is depicted.

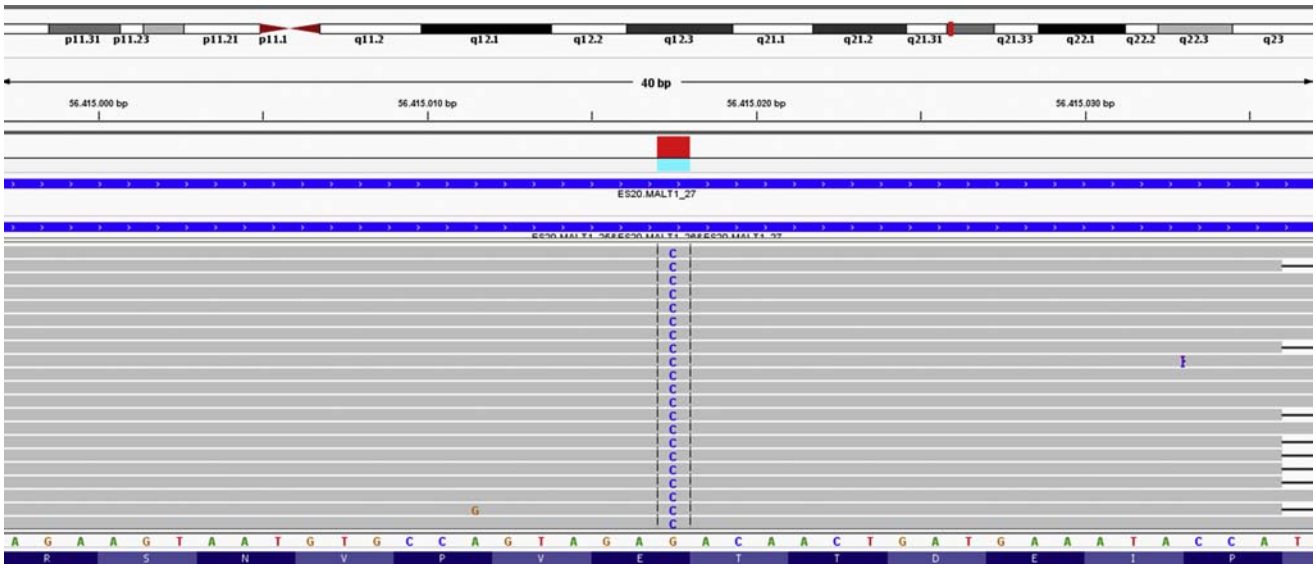

FIG E2. Result of targeted next-generation sequencing analysis of a blood sample from the patient showing homozygous c.2418G>C missense mutation in *MALT1* gene leading to Glu806Asp (E806D) exchange in MALT1A.

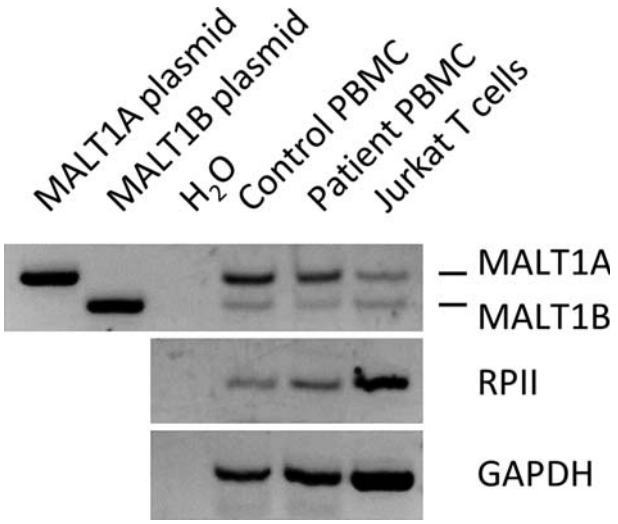

FIG E3. Analysis of MALT1 isoform expression by RT-PCR in PBMCs isolated from the blood of the patient and from a healthy control by using exon 6 and exon 9/10 primers amplifying both isoforms. Jurkat T cells, as well as MALT1A or MALT1B plasmid DNA, served as controls. Fragments for MALT1A (146 bp) and MALT1B (113 bp) are indictated. GAPDH and RNA polymerase II (RPII) amplification were used as controls.

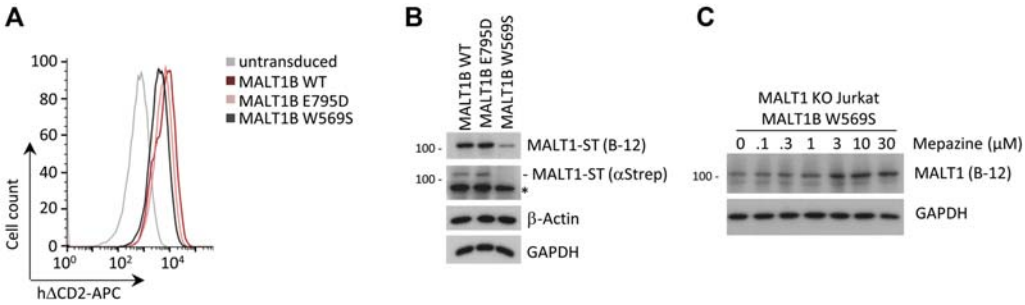

FIG E4. A, Transduction efficiency of MALT1 KO;NF-κB–EGFP Jurkat T cells with ST-tagged MALT1 WT, E795D, and W569S mutants was monitored by coexpression of the surface marker hΔCD2 in fluorescence-activated cell sorting. **B,** Protein expression of MALT1B WT and mutant proteins were assessed by Western blot using MALT1 and StrepMAB antibodies. Asterisk marks an unspecific band. **C,** Jurkat T cells expressing MALT1B W569S were incubated for 5 hours with increasing concentrations of the allosteric MALT1 inhibitor S-mepazine, and MALT1 protein stabilization was assessed by Western blotting. *APC*, Allophycocyanin.

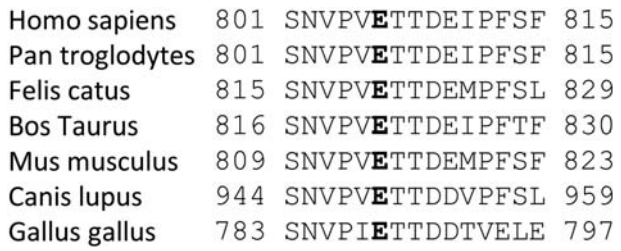

FIG E5. Evolutionary conservation of MALT1A E806 among different species.

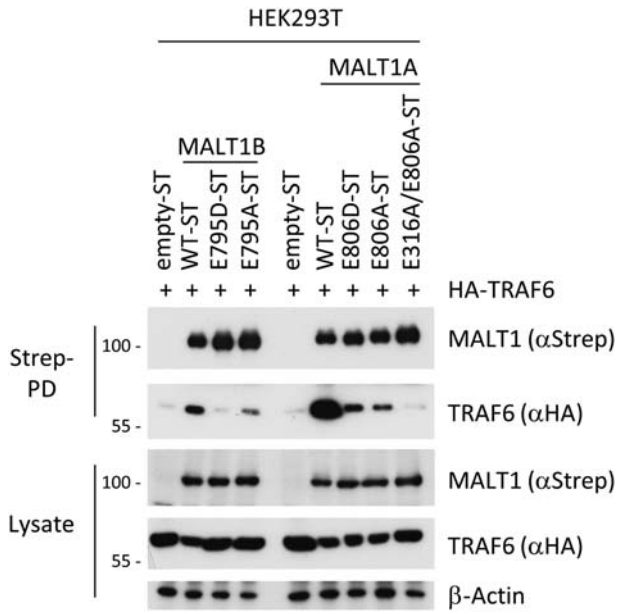

FIG E6. HEK293 cells were transfected with HA-TRAF6 and MALT1-FlagStrepII WT and mutant constructs. Streptactin-pulldown (Strep-PD) was performed and MALT1-ST and HA-TRAF6 binding was analyzed by Western blot.

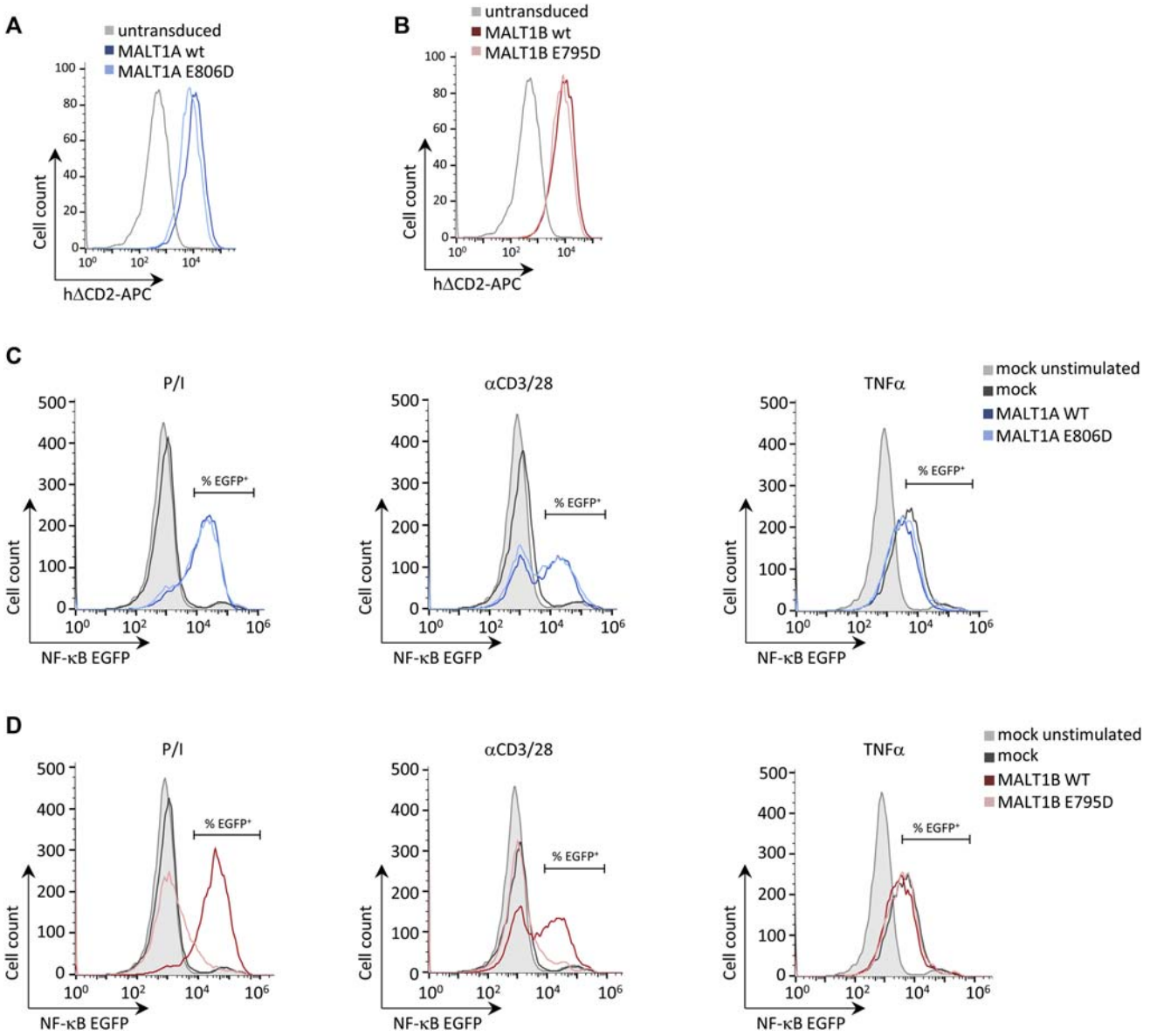

FIG E7. **A** and **B,** Transduction efficiency of MALT1 KO;NF-κB–EGFP Jurkat T cells with MALT1A (**A**) and MALT1B (**B**) WT and mutant constructs was monitored by coexpression of surface marker hΔCD2 in fluorescence-activated cell sorting. **C** and **D**, Induction of the NF-κB–EGFP reporter in MALT1 KO Jurkat T cells after transduction of mock, MALT1A WT, MALT1A E806D, MALT1B WT, and MALT1B E795D as determined by fluorescence-activated cell sorting after P/I, αCD3/CD28, or TNF-α stimulation. Gate depicts the EGFP-positive cells used for quantification in Fig 1, *G* and *H*. *APC*, Allophycocyanin.